ELSEVIER

Journal of Nuclear Materials 289 (2001) 194–198

journal of nuclear materials

www.elsevier.nl/locate/jnucmat

Determination of the defect creation mechanism in fluoroapatite

Stéphane Soulet [a,b], Jacques Chaumont [a,*], Jean-Claude Krupa [c], Joëlle Carpena [b], Marie-Odile Ruault [a]

[a] *Centre de Spectrométrie Nucléaire et de Spectrométrie de Masse, CNRS-IN2P3, F-91405 Orsay Campus, France*
[b] *CEA-Cadarache, DESD/SEP/LEMC, 13108 Saint-Paul-lez-Durance, France*
[c] *Institut de Physique Nucléaire, CNRS-IN2P3, 91406 Orsay Cedex, France*

Abstract

Most of strategies to immobilize actinides are concerned with their incorporation in dedicated solid matrices for a long disposal-time. Chemical durability of these matrices is a major problem. Radiation damages due to α-decay events can strongly reduced it. The defect creation mechanism has been determined in fluoroapatite using a transmission electron microscope (TEM) on line with an ion implanter. At room temperature, the defect creation is controlled by amorphization directly in the cascade. From this result and published data on the defect annealing in this material, the disorder evolution as a function of time has been established. An application concerning the incorporation of ^{244}Cm is considered.

PACS: 23.60.+e; 61.72Cc; 61.80.Az

1. Introduction

Actinides are very radiotoxic elements that often have long life-times. Their incorporation in dedicated ceramics for long time in a deep stabilized geologic repository is one strategy under investigation to isolate them from the biosphere. Several previous studies describe the apatitic structure as a crystalline phase of interest for nuclear waste storage [1–7]. The most abundant apatite chemical composition found in nature is fluoroapatite ($Ca_{10}(PO_4)_6F_2$). The general aim of this work is to study the radiation effects from actinides in this crystalline phase.

During α-decay events, energetic recoil nuclei (α-recoils) may induce a large disorder level or even a crystalline to amorphous phase transition. This phase transformation has two effects:

(i) The water dissolution rate is increased by a factor up to 100 [8].
(ii) In case of multiphase matrices or inhomogeneous actinide concentrations, the associated macroscopic swelling [8] can induce micro-fractures or even a partitioning of the waste form which may enhance the actinide release by another factor since the leached surface area increases.

During the disposal time, a waste form will undergo a significant radiation dose that is often expressed as the number of displacements per atom (dpa), which is generally one to two orders of magnitude larger han the dose necessary to amorphize it, depending on the actinide loading. As a consequence, if no precaution is taken, total amorphization can occur during disposal thus leading to a large increase of the actinide release. Consequently, waste forms should ideally have some efficient recovery mechanisms to prevent total amorphization. But the safest disposal conditions are even more strict. Indeed, when the disorder increases, a percolation phenomenon may appear between the disordered zones, leading to accelerated dissolution paths deep inside the waste form and hence to a large increase of the leachable

* Corresponding author. Tel.: +33-1 69 15 52 88; fax: +33-1 69 15 52 68.
E-mail address: chaumont@csnsm.in2p3.fr (J. Chaumont).

0022-3115/01/$ - see front matter
PII: S0022-3115(00)00697-8

surface area [9]. The disorder concentration should remain below about 20% or 30% to avoid this defect percolation effect. Then it is obvious that the disorder level in the waste forms must be predicted at any disposal time to fulfill this condition. For this reason, the creation and annealing rates of the defects induced by α-recoils in the waste form have to be measured to determine the disorder evolution. The defect annealing rates have been measured on fluoroapatite single crystals by Rutherford Backscattering Spectrometry associated with channeling (RBS-C). These experiments have shown that a very important defect recovery process exists due to the electronic energy loss of α-particles [10,11], and on the other hand, the thermal annealing is very low and usually negligible compared to α-annealing [9,11]. This paper is devoted to the determination of the defect creation mechanism in fluoroapatite. From our results and published data on the defect annealing behavior [10,11], the differential equation which governs the disorder evolution as a function of time was established in fluoroapatite [9]. An example of numerical evaluation concerning the incorporation of 1% weight of ^{244}Cm is considered.

2. Experimental techniques

Disorder induced by α-recoils are simulated by ion-beam irradiation in this study. The disorder evolution as a function of ion fluence is measured to determine the defect creation rate. For this measurement, RBS-C cannot be used in fluoroapatite due to the very efficient α-annealing effect that anneals the defects created by ion-simulated α-recoil [10]. Consequently, the disorder creation was measured using a 120 kV transmission electronic microscope (TEM) on line with the 190 kV IRMA implanter [12,13]. TEM fluoroapatite samples have been prepared from a sintered polycrystalline disc [14]. This disc is thinned down to a 200 μm thickness and carefully polished on one face with different diamond powder suspensions down to a grain size of 0.25 μm. The other face is thinned to a bowl shape down to about a 5 μm thickness at the center. An argon ion mill was used to thin the sample to preforation.

The 100 keV α-recoils are simulated at room temperature by 320 keV Pb-ions. This energy has been chosen because it does not modify the defect nature and allows for increasing the disordered layer thickness which improves the signal over noise ratio. The ion current used is set as low as 0.05 μA/cm^2 to keep the ion-beam heating effect at a negligible level. Irradiations have been performed by steps of 10^{13} Pb/cm^2. After each irradiation the disorder level is measured using the selected area electron diffraction technique (SAED) on several zones in order to improve the accuracy.

Five conditions must be fulfilled to compare the different SAED patterns obtained during in situ experiment [15]:

(i) It is necessary to work with the same crystalline orientation far from any low index axis to avoid large variations of the electron fraction that produces the diffuse halo [16,17].

(ii) As the sample has an inhomogeneous thickness, each measurement must be performed with the same electron-beam spot size and with the same position on the sample to keep constant the crystalline fraction of the selected area.

(iii) The electron beam current of only 0.5 nA was spread on a 50 μm^2 area to limit the defect annealing by the analyzing electrons [18,19]. Under these conditions, the required time to come back on a given position and to take a picture is about 1 min; thus the electron annealing effect corresponds to less than 1% of defects that are present.

(iv) The diffraction patterns are registered on photographic plates with always the same exposure time (Fig. 1). To make correction for any electron-beam current drift, its intensity is measured precisely with a Faraday cup before each SAED measurement.

(v) All the plates corresponding to a given position on the sample must be developed simultaneously to prevent any perturbations due to the developer temperature and age.

Fig. 1. Diffraction pattern after 2×10^{13} Pb/cm^2 implantation. The diffuse ring due to the electron diffraction on the amorphous zones and the diffraction maximum due to the crystalline remaining part are displayed.

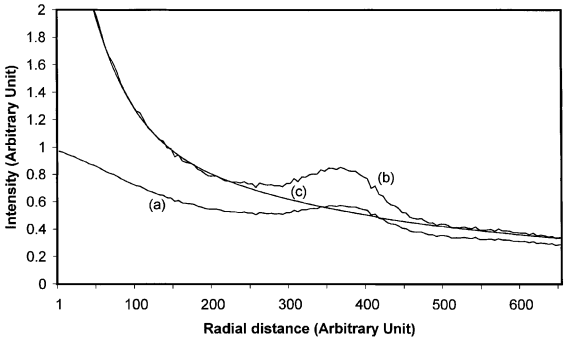

Fig. 2. Typical diffuse ring intensity profile: (a) as measured, (b) after correction for photographic plate nonlinearity, and (c) background fit.

The plates are then digitized to measure the intensity of the diffuse ring produced by the electron diffraction on the amorphous zones. The intensity profile is measured along four different radial directions chosen where there are no diffraction maximum. Each intensity profile is corrected to account for the nonlinear response of the plates [15] (Fig. 2). The diffuse ring appears on a background that varies rapidly. A good fit of this background can be obtained on both side of the diffuse ring using the sum of two exponentials and a constant term [15] (Fig. 2). Its subtraction gives us the ring intensity. The average of the results on the four radii is used to define the disorder level after each irradiation step.

3. Experimental results

During the first Pb-ion irradiation the thinnest parts of the TEM sample are destroyed. Therefore, a large fraction of the zones investigated provides a thickness that can be larger than the Pb-ion range. Thus, the diffuse ring intensity, which is proportional to the total disorder volume, corresponds to a very inhomogeneous defect distribution versus depth since a fraction of the sample thickness always remains crystalline. The measured intensity as a function of Pb-ion fluence gives the evolution of an average disorder level over zones having different defect concentrations. It is thus difficult to get from these measurements a very precise value for the defect creation rate and the amorphization dose. However, the experimental data as a function of Pb-ion fluence (Fig. 3) can be fitted by Eq. (1)

$$y = 1 - \exp(-V\Phi/R), \tag{1}$$

where y is the disorder fraction when there is no defect post-cascade annealing, Φ the ion fluence, V the average amorphized volume by each ion impact, and R is the average amorphized thickness. The fit is consistent with the fluoroapatite amorphization being governed by the direct-impact model [20,21]. When this amorphization process is dominant every ion creates a small-localized amorphous volume in the virgin part of the crystal. This volume, which depends on the temperature, defines the defect creation rate.

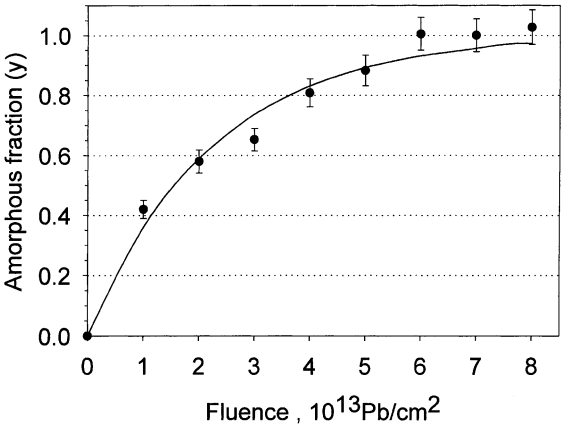

Fig. 3. Amorphization curve of $Ca_{10}(PO_4)_6F_2$ as a function of lead ion fluence. The solid line is obtained using Eq. (1).

Eq. (1) fit provides a V/R ratio equal to $(4.5 \pm 0.3) \times 10^{-14}$ cm^2. From a SRIM calculation [22] the amorphized thickness R is determined to be to 73 ± 4 nm. Thus, the amorphous volume created by each lead ion is equal to $(3.3 \pm 0.4) \times 10^{-19}$ cm^3.

4. Application for actinide immobilization

The present results, showing that the fluoroapatite amorphization occurs according to the direct impact model, allow the use of the differential equation established by Chaumont et al. [9] to calculate the matrix disorder level evolution, y, as a function of time in the case of fluoroapatite

$$\mathrm{d}y = V_0(T)[1-y]\mathrm{d}D - y[F\exp(-E_a/kT)\mathrm{d}t + (c(T)E_\alpha/2)\mathrm{d}D]. \tag{2}$$

This equation contains:

(i) The disorder creation term, $V_0(T)$, which is the average disordered volume produced by a α-recoil at temperature, T, $(1-y)$ is the crystalline fraction and $\mathrm{d}D$ is the dose increment.

(ii) The defect thermal annealing term, which depends on temperature and is defined by F the jump frequency and E_a the activation energy. This thermal annealing term should be proportional to the surface of the crystalline/amorphous interface. This surface cannot be precisely calculated since the shape of individual defects is not known, but after some time a more or less steady size distribution

will probably appear. Consequently, as a first approximation, we will assume that the thermal annealing term is proportional to y.

(iii) The α-annealing term, $c(T)$, which is the volume recovery per electronvolt deposited by the α-particles having an energy E_α. When α-annealing operates the disordered fraction, y, decreases according to a mono-exponential law as a function of the α_flux [10]. It means that the annealing effect, dy, is always proportional to y and that only the energy deposited into the amorphous zones is efficient.

This differential equation can only be partially solved using the initial conditions: $y = 0$ and $D = 0$ at $t = 0$. It gives rise to Eq. (3) where the amorphous fraction, y, appears as a function of the cumulative dose, D

$$y = A[1 - (F\exp(-E_a/kT)I(t) + 1)\exp(-(V_0(T) + c(T)E_\alpha/2)D - F\exp(-E_a/kT)t)]$$

with

$$A = V_0(T)/(V_0(T) + c(T)E_\alpha/2)$$

and

$$I(t) = \int_0^t \exp[(V_0(T) + c(T)E_\alpha/2)D + F\ \exp(-E_a/kT)u]\,du. \quad (3)$$

More details on this equation will be published elsewhere [9].

When actinides are introduced into fluoroapatite, a chemical composition modification is necessary to keep the charge balance. To apply Eq. (2), one assumes that for low actinide concentrations this chemical modification does not change the defect creation and annealing rates. This equation was solved in case of a fluoroapatite matrix loaded with 1 wt% of ^{244}Cm ($t_{1/2} = 18.1$ years, $E_\alpha = 5.8$ MeV) which decays successively to ^{240}Pu ($t_{1/2} = 6570$ years, $E_\alpha = 5.18$ MeV) and ^{236}U ($t_{1/2} = 2.4 \times 10^7$ years) which was considered as stable in the present application.

The disorder volume produced by a 95 keV recoiling ^{240}Pu atom at room temperature has been calculated from the disordered volume produced by 320 keV lead ion assuming that both volumes are proportional to the respective number of displaced atoms obtained by SRIM calculation [22]. This volume is equal to 1.2×10^{-19} cm^3, while previous RBS measurements give a V_0 value of 4.8×10^{-20} cm^3 [9]. Presently, it is difficult to know which method gives the more accurate result. To calculate the disorder level evolution, an average value of $V_0 = 8.4 \times 10^{-20}$ cm^3 was used.

In the beginning of the disposal time, the waste form temperature will be higher than 25°C, the temperature where $V_0(T)$ has been measured. Taking into account the fact that the amorphization dose is inversely proportional to $V_0(T)$ when the direct-impact model applies, the published curves giving the amorphization critical dose evolution with respect to temperature for the fluoroapatite [23,24] can be used to evaluate the amorphous volume reduction with the temperature rise. Presently, the repository temperature evolution is not yet well determined. If one considers a constant temperature of 60°C, an increase of 25% in the critical amorphization dose can be expected with respect to 25°C data [23,24]. Consequently, V_0 is effectively decreased by a factor 1.25: V_0 (60°C) $= 6.7 \times 10^{-20}$ cm^3. For the annealing terms, previous evaluations give at 60°C a defect thermal lifetime of 1 million years [25] and a recovery volume per electronvolt equal to 1.16×10^{-25} cm^3/eV [9,10].

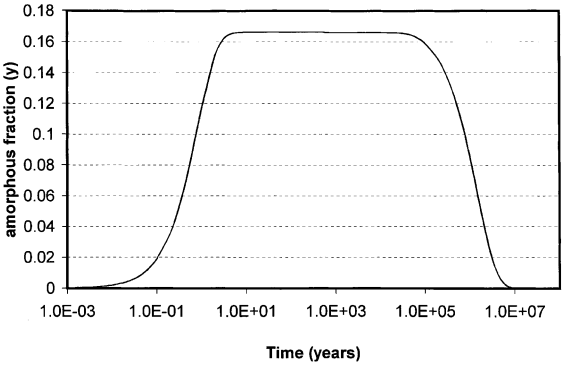

Fig. 4. Disorder level evolution as a function of time for a fluoroapatite matrix loaded with 1 wt.% of ^{244}Cm at 60°C.

From these data, the disorder evolution versus time in fluoroapatite can be calculated. It is plotted in Fig. 4. This curve shows that the disorder level increases rapidly up to about 17% and then reaches a plateau lasting 10^5 years that ends when the α-activity becomes negligible and the thermal annealing operates. There is no significant variation of the disorder level when the ^{244}Cm is replaced by its daughter ^{240}Pu with a lower α-energy, since the recoiling atom energy is reduced in the same proportion.

5. Conclusion

The first result of this study is that the amorphization process in $(Ca_{10}(PO_4)_6F_2)$ fluoroapatite follows the direct-impact model. This amorphization mechanism has already been reported for a ^{244}Cm loaded silicate apatite: $Ca_2Nd_8(SiO_4)_6O_2$ [8,26]. Thus, this study confirms that direct-impact amorphization is the dominant process for a large range of apatite compositions.

The second result is that in a fluoroapatite potential matrix, the disorder induced by α-recoils rapidly reaches an equilibrium low level that is independent of the dose

rate. This property is due to the very efficient annealing effect produced by the α-particle flux.

However, the chemical composition of the phosphocalcic fluoroapatite must be modified to introduce in the structure a significant amount (10% weight) of actinides.

Experiments are in progress to determine the influence of this modification on the defect creation and annealing rates.

Acknowledgements

We gratefully acknowledge the assistance of the technical staff of the SEMIRAMIS team. We are indebted to S. Gautrot and O. Kaitasov who performed the lead implantation. This work is a part of the PhD studies of S. Soulet who is supported by the French Commissariat à l'Energie Atomique.

References

[1] J. Carpena, J.L. Lacout, French Patent No. 93 08676, 1993.
[2] R.C. Ewing, W.J. Weber, W. Lutze, in: E.R. Merz, C.E. Walter (Eds.), Disposal of Weapons Plutonium, Kluwer Academic Publications, Netherlands, 1996.
[3] J. Carpena, L. Boyer, J.L. Lacout, French Patent No. 98 11334, 1998.
[4] J. Carpena, V. Sere, J.R. Kienast, Proc. Migration '95, St-Malo, France, 1995.
[5] V. Sere, PhD thesis, University of Paris VII, 1995.
[6] R. Bros, J. Carpena, V. Sere, A. Beltritti, Radiochim. Acta 74 (1996) 277.
[7] J. Carpena, CEA Internal Report, NT-SESD 92-21, 1992.
[8] W.J. Weber, R.C. Ewing, C.R.A. Catlow, T. Diaz de La Rubia, L.W. Hobbs, C. Kinoshita, H. Matzke, A.T. Motta, M.A. Nastasi, E.H.K. Salje, E.R. Vance, S.J. Zinkle, J. Mater. Res. 13 (1998) 1434.
[9] J. Chaumont, S. Soulet, J.C. Krupa, J. Carpena, to be published.
[10] S. Ouchani, J.-C. Dran, J. Chaumont, Nucl. Instr. and Meth. B 132 (1997) 447.
[11] S. Ouchani, PhD thesis, University of Paris XI, 1997.
[12] J. Chaumont, F. Lalu, M. Salomé, A.M. Lamoise, H. Bernas, Nucl. Instr. and Meth. B 9 (1981) 344.
[13] M.O. Ruault, J. Chaumont, H. Bernas, Nucl. Instr. and Meth. B 209&210 (1983) 351.
[14] N. Sénamaud, D. Bernache-Assollant, E. Champion, M. Heughebaert, C. Rey, Solid State Ionics 101–103 (1997) 1357.
[15] S. Soulet, J. Carpena, J. Chaumont, O. Kaitasov, J.C. Krupa, to be published.
[16] M. Schack, PhD thesis, University of Paris XI, 1984.
[17] A. Traverse, M.O. Ruault, L. Mendoza-Zelis, M. Schack, H. Bernas, J. Chaumont, in: S.T. Picraux, W.J. Choyke (Eds.), Metastable Materials Formation by Ion Implantation, Elsevier, Amsterdam, 1984.
[18] A. Meldrum, L.A. Boatner, R.C. Ewing, in: Proceedings of the MRS Symposium, vol. 439, 1996.
[19] A. Meldrum, L.A. Boatner, R.C. Ewing, J. Mater. Res. 12 (7) (1998) 1816.
[20] J.F. Gibbons, Proc. IEEE 60 (1972) 1062.
[21] G. Carter, R. Webb, Radiat. Eff. Lett. 43 (1979) 19.
[22] J.F. Ziegler, J.P. Biersack, D.J. Marwick, The Stopping and Range of Ions in Matters, SRIM-2000, IBM Corporation, New York.
[23] R.C. Ewing, L.M. Wang, W.J. Weber, Proc. Mat. Res. Soc. 373 (1995) 347.
[24] L.M. Wang, M. Cameron, W.J. Weber, K.D. Crowley, R.C. Ewing, in: P.W. Brown, B. Constantz (Eds.), Hydroxyapatite and Related Materials, CRC Press, Boca Raton, vol. 243, 1994.
[25] R.L. Fleischer, P.B. Price, R.M. Walker, Nuclear Tracks in Solids, University of California Press, Berkeley, CA, 1975.
[26] W.J. Weber, R.C. Ewing, A. Meldrum, J. Nucl. Mater. 250 (1997) 147.